Effects of knot tightness at the molecular level

Liang Zhang[a,b], Jean-François Lemonnier[b], Angela Acocella[c], Matteo Calvaresi[c], Francesco Zerbetto[c,1], and David A. Leigh[a,b,1]

[a]School of Chemistry and Molecular Engineering, East China Normal University, 200062 Shanghai, China; [b]School of Chemistry, University of Manchester, M13 9PL Manchester, United Kingdom; and [c]Dipartimento di Chimica "G. Ciamician", Università di Bologna, 40126 Bologna, Italy

Edited by Michael L. Klein, Institute of Computational Molecular Science, Temple University, Philadelphia, PA 19122, and approved December 18, 2018 (received for review September 8, 2018)

Three 8_{19} knots in closed-loop strands of different lengths (~20, 23, and 26 nm) were used to experimentally assess the consequences of knot tightness at the molecular level. Through the use of ^{1}H NMR, diffusion-ordered spectroscopy (DOSY), circular dichroism (CD), collision-induced dissociation mass spectrometry (CID-MS) and molecular dynamics (MD) simulations on the different-sized knots, we find that the structure, dynamics, and reactivity of the molecular chains are dramatically affected by the tightness of the knotting. The tautness of entanglement causes differences in conformation, enhances the expression of topological chirality, weakens covalent bonds, inhibits decomplexation events, and changes absorption properties. Understanding the effects of tightening nanoscale knots may usefully inform the design of knotted and entangled molecular materials.

molecular knots | supramolecular chemistry | chemical topology

Knots are found in some proteins (1), linear and circular DNA (2), and polymers of sufficient length and flexibility (3). The strand entanglements affect molecular size (4), stability (5), and various mechanical properties (6–8), although much of the understanding as to how and why remains unclear. To date the influence of various structural traits, such as the number of knot crossings (9), writhe (10), backbone crossing ratio (BCR) (11), and the global radius of curvature (12), on properties has mainly been studied by simulations (13–16) rather than experiment (17, 18). Knot tightness (19–21) is a particularly easy-to-appreciate characteristic, familiar from our everyday experience in the macroscopic world, that may also have significant effects at the molecular level (4, 22–27). Long polymers are predicted to have knotted regions that are both frequent and tight (25). The tightness of knotting is implicated in variations in the thermostability of entangled proteins (26) and is thought to have consequences for tensile strength (27). However, it is difficult to assess intrinsic effects of knotting by comparing structures with rather different chemical compositions. Monodispersed synthetic molecular knots are ideal models through which to evaluate the influence of knot tightening on physical and chemical properties (17, 18). Here we report experimentally determined property differences in a set of three knotted molecules that differ only in the length of flexible regions (alkyl chains) that separate more rigid sections (composed of aromatic rings) of the strand. Using a braiding strategy previously used to assemble (28) an extremely tightly knotted 192-atom loop 8_{19} knot (**1**) (29), the alkene-terminated chains used to close the knotted structure were extended without otherwise altering the outcome of the knot synthesis (Fig. 1). This resulted in a set of three 8_{19} molecular knots that differ only in the length of the alkyl chains in the loop (**1** is 192 atoms long, **2** is 216 atoms long, and **3** is 240 atoms long, a 25% variation in strand length involving only the flexible regions). We probed the properties of the different-sized knots by ^{1}H NMR spectrometry, mass spectrometry, UV spectroscopy, and circular dichroism, and used computational studies to help explain the role the increasing tightness of knotting plays in altering physical and chemical behavior.

Ligand strands **L1**–**L3** bearing Tris(2,2′-bipyridine) motifs with different lengths of alkene-terminated alkyl chains were prepared by analogy to that previously used to prepare **1** (29). Treatment of the ligands with equimolar amounts of $FeCl_2$, followed by ring-closing metathesis (30), gave the corresponding 8_{19} knot complexes $[Fe_4\mathbf{Knot}](PF_6)_8$ (**Knot** = **1**–**3**; Fig. 1) which were isolated and characterized by electrospray ionization mass spectrometry and ^{1}H NMR spectroscopy (*SI Appendix*, Figs. S1–S8). The ^{1}H NMR spectra of the three knotted complexes are essentially superimposable (*SI Appendix*, Figs. S14 and S15), other than the alkyl region due to the differences in chain length, indicating that metal coordination of the knotted ligands holds the three complexes in similar conformations. Subjecting the metallated knots to a 1:1 MeCN/$NaOH_{aq}$ (1 M) solution at 80 °C, followed by size-exclusion chromatography, afforded the corresponding demetallated knots **1**–**3** with different degrees of tightness (Fig. 1 and *SI Appendix*, Figs. S9–S12). The BCRs (11) of **1**–**3** are 24, 27, and 30, respectively. The diffusion coefficients (D) values of the three knots were measured by diffusion-ordered spectroscopy experiments; the relative effective hydrated radius of the knots increases by 8% from **1** to **2** and 16% from **2** to **3** in line with the 12.5% and 25% increase in the length of the flexible regions, respectively (*SI Appendix*, Figs. S19–S21). The optimized reaction times used in the demetallation process were 15 min for $[Fe_4\mathbf{1}](PF_6)_8$ (resulting in a 35% yield of **1**), 10 min for $[Fe_4\mathbf{2}](PF_6)_8$ (43% yield of **2**), and less than 5 min for $[Fe_4\mathbf{3}](PF_6)_8$ (65% yield of **3**). The differences in reactivity (yield and reaction time) can be rationalized by loosening of the knot giving the strand significantly greater flexibility, particularly after displacement of the first iron cation. This makes it easier for hydroxyl ions to access the remaining iron centers (31), decreasing the amount of the poorly soluble iron bipyridine hydroxide by-products (32) that reduce the yield of metal-free knot.

Significance

Knots and entanglements occur in proteins, DNA, and synthetic polymers and are being used to form the basis of interwoven nanomaterials. Understanding how the tautness of molecular entanglements affects properties is crucial for the future design of knotted, woven, and entangled molecules and materials. However, while there are many theoretical studies on such systems there are very few experimental studies. Here we investigate the influence of knot tightness in a range of physical and chemical properties for three knots tied in 20-, 23-, and 26-nm closed-loop strands. We find that the tightness of the molecular knots significantly affects reactivity, conformation, and the expression of chirality.

Author contributions: L.Z., F.Z., and D.A.L. designed research; L.Z., J.-F.L., A.A., M.C., and F.Z. performed research; A.A., M.C., and F.Z. analyzed data; and L.Z., J.-F.L., A.A., M.C., F.Z., and D.A.L. wrote the paper.

The authors declare no conflict of interest.

This article is a PNAS Direct Submission.

[1]To whom correspondence may be addressed. Email: francesco.zerbetto@unibo.it or david.leigh@manchester.ac.uk.

This article contains supporting information online at www.pnas.org/lookup/suppl/doi:10.1073/pnas.1815570116/-/DCSupplemental.

Published online January 25, 2019.

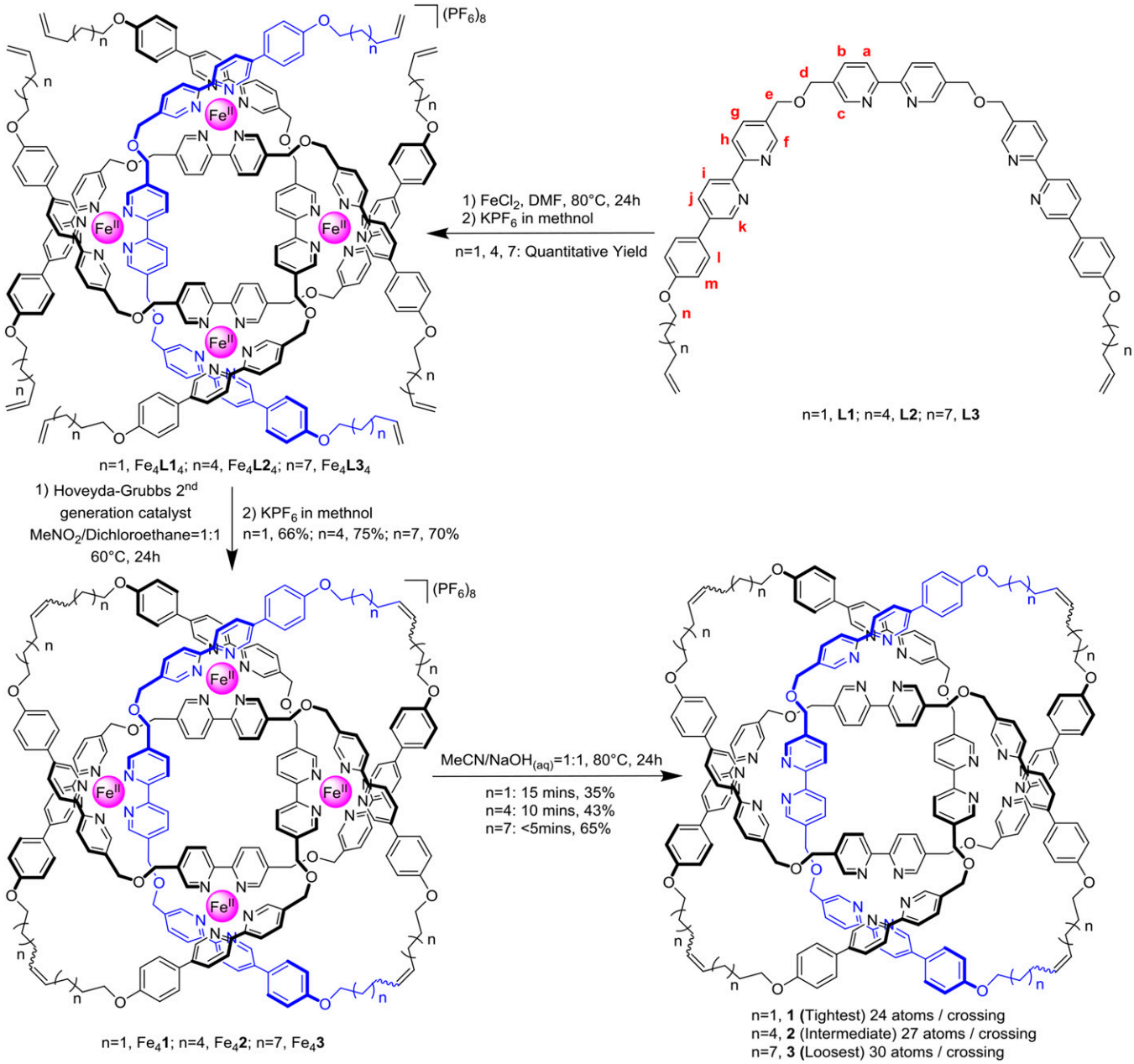

Fig. 1. Synthesis of $[Fe_4Knot](PF_6)_8$ (Knot = **1–3**) and their subsequent demetallation to 8_{19} knots **1–3**.

The yields of the demetallated 8_{19} knots did not increase with longer reaction times.

In contrast to the similar chemical environments observed for the protons of the metallated knots, the ^{1}H NMR spectra of **1–3** differ markedly from each other in several regions (Fig. 2). Methylene (CH_2) groups H_d and H_e in the tightest knot, **1**, appear as multiplets because the constricted chiral environment accentuates their diastereotopicity. With the loosening of the knot from **1** to **2**, the signals of H_d and H_e broaden, becoming a single broad signal (at 600 MHz in $CDCl_3$) in **3** in line with the protons occupying less-constricted, less well-defined, environments (Fig. 2*C*). Variable-temperature ^{1}H NMR spectra of **1–3** show little change over a large temperature range (238–318 K), indicating that the variances in the ^{1}H NMR spectra of the three knots are primarily due to the differences in tightness affecting conformation and not general dynamic phenomena (*SI Appendix*, Figs. S16–S18).

The resonances of the aromatic protons in the looser knots, **2** and **3**, shift to low field, their chemical shifts moving closer to those of the corresponding building blocks (**L2** and **L3**). The shielding of H_d, H_e, H_f, and H_k, in particular, are intermediate between that of the corresponding protons in **1** and **3**. Concomitantly, the resonances of most of the alkyl protons (e.g., H_n) move upfield. Both effects are consistent with a loss of π–π interactions in the tightly knotted structures and the rise of CH–π interactions between the alkyl protons and aromatic motifs in the looser knots (Fig. 2*B* and *SI Appendix*, Fig. S22 and Table S1). It suggests that the conformation of the tightest knot, **1**, is stabilized by π–π stacking with the aromatic groups involved in the entangled region of the structure with the alkyl chains to the outside. In **2** and **3**, the longer alkyl chains slip into the knotted region while the aromatic groups move to the periphery, thus generating fewer π–π interactions but more CH–π interactions. These

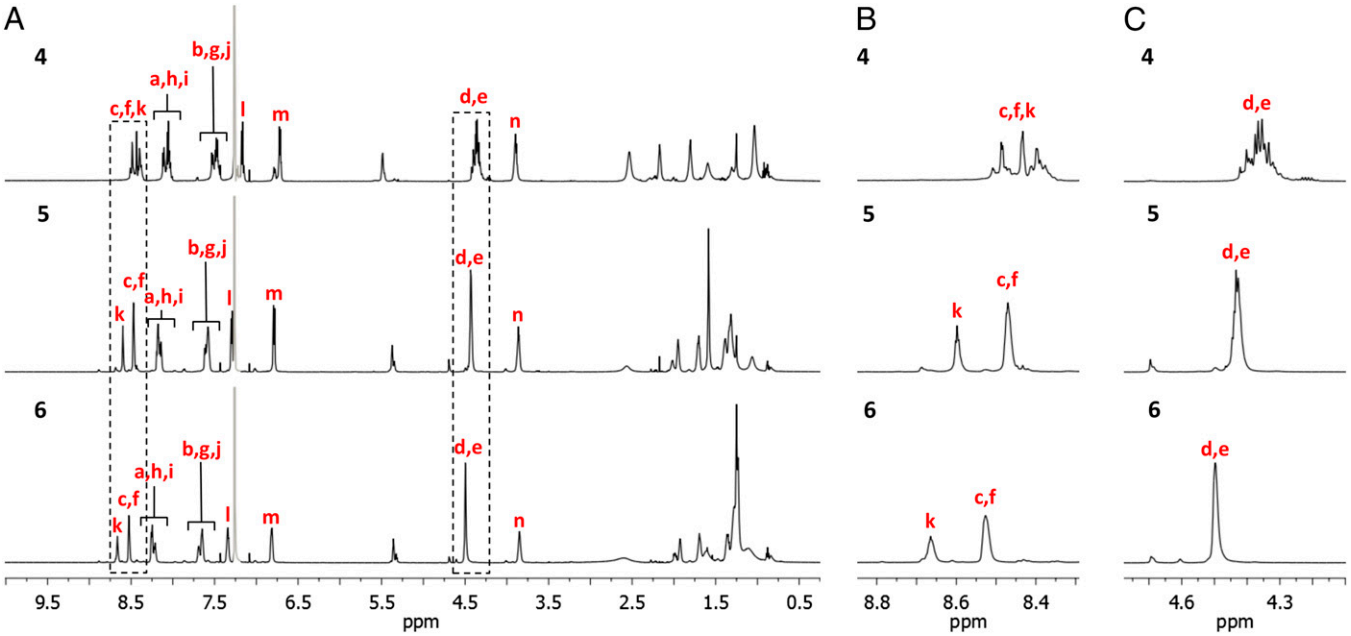

Fig. 2. Partial ^{1}H NMR spectra (600 MHz, $CDCl_3$, 298 K) of 8_{19} knots **1**, **2**, and **3**; (*A*) region 0.25–10.0 ppm. (*B*) Expanded regions 8.3–8.8 ppm. (*C*) Expanded regions 4.1–4.7 ppm. Residual solvent peaks are shown in gray. The lettering corresponds to the proton labeling in Fig. 1.

observations provide experimental evidence in support of the migration of entanglements from rigid to flexible regions, behavior that has been predicted in simulations of knotted polymers (33, 34).

To help explain the experimental data, molecular-dynamics calculations were performed on **1–3**. The starting geometries were based on the X-ray structure of the metallated knot $[Fe_4\mathbf{1}](PF_6)_7Cl$ (29), removing the iron cations and counteranions, and increasing the chain length for **2** and **3**. A summary of the dynamics in terms of principal component analysis (PCA) maps is shown in Fig. 3 *A*–*C*. (For illustrative examples of populated conformations during the simulations, see *SI Appendix*, Figs. S32–S34.) The tightest knot **1** shows markedly different dynamics with respect to knots **2** and **3** and is locked into

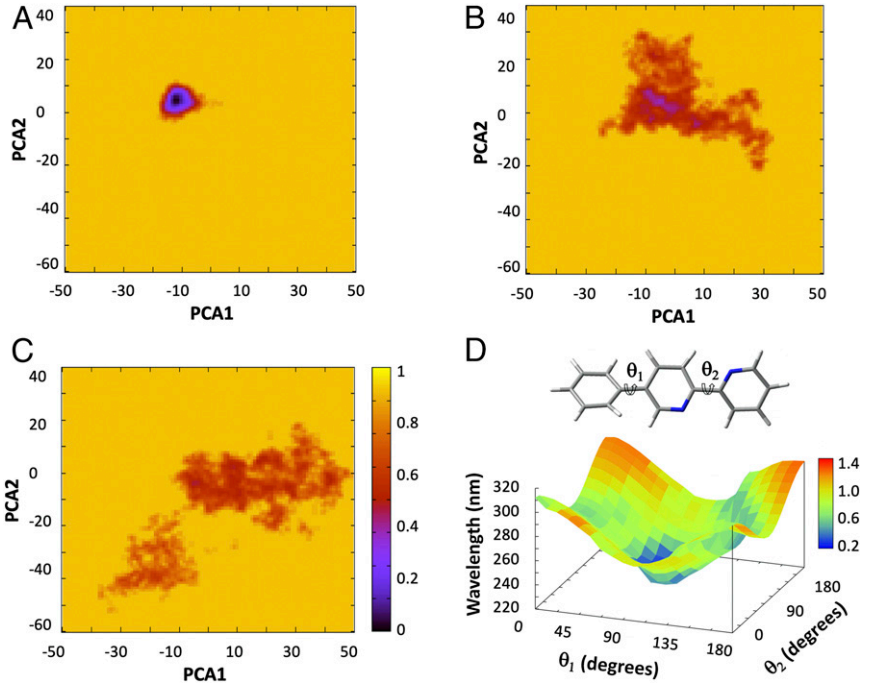

Fig. 3. Normalized free energy surfaces, according to PCA of (*A*) knot **1**. (*B*) Knot **2** and (*C*) knot **3**. The *x* and *y* axis are displacement vectors spread over the entire system, i.e., how much each atom "moves." They are calculated with respect to an average structure (physically meaningless) and can be thought of directions of flexibility. (*D*) TD-DFT (M06-2X/6–31G*) calculated four-dimensional plot of θ_1 and θ_2 together with the associated wavelength of excitation and the oscillator strength (in color scale of the phenyl-bipyridine fragment).

essentially a single conformation stabilized by strong π–π interactions that involve every aromatic ring (Fig. 3*A* and *SI Appendix*, Fig. S32). The knot of intermediate tightness, **2**, populates a larger variety of conformations in which π–π interactions are limited (Fig. 3*B* and *SI Appendix*, Fig. S33), while the loosest knot, **3**, has no particularly preferred conformation (Fig. 3*C* and *SI Appendix*, Fig. S34). The Tris(2,2′-bipyridine) units, the most rigid part of the structure, largely move out of the entangled region—and the alkyl chains, the more flexible region, move into it—in most of the thermally equilibrated conformations of the loosest knot, **3**. This is consistent with the experimentally observed ^{1}H NMR shifts and illustrates how local flexibility of the strand affects both conformation and the position of the entanglement. The results of both experiment and simulation indicate that the dynamic properties of the 8_{19} knots are profoundly influenced by the tightness of the entanglements.

To evaluate the effect of knot tightness on covalent bond strengths, tandem mass spectrometry (MS-MS) experiments were conducted on the $[M + 2H]^{2+}$ peak (Fig. 4 *A, C*, and *E*) of knots **1–3** activated by collision-induced dissociation (CID). This resulted in multiply charged ions with a loss of mass consistent with covalent bond scission and subsequent unraveling of the knotted strand (Fig. 4 *B, D*, and *F*). Upon increasing the normalized collision energy in 1-eV steps until bond cleavage occurred, the looser knots (**2** and **3**) required significantly higher energies (35 and 55 eV, respectively) to fragment than **1** (28 eV). For each knot scission always occurs at the carbon–oxygen bond between the central bipyridine and phenyl–bipyridine units, but the knots showed two distinct types of fragmentation pattern (type I, Fig. 4*G* and type II, Fig. 4*H*). For the tightest knot **1**, fragmentation (loss of a water molecule; m/z = 1,681.75) is followed by loss of an adjacent central bipyridine unit (m/z = 1,582.67; Fig. 4*B*, type I). In contrast, the loosest knot **3** requires a minimum of 55 eV to fragment and directly forms two breakdown products that each contain half of the knot (m/z = 2,008.36 and 1,810.45; Fig. 4*F*, type II). Both types of fragmentation

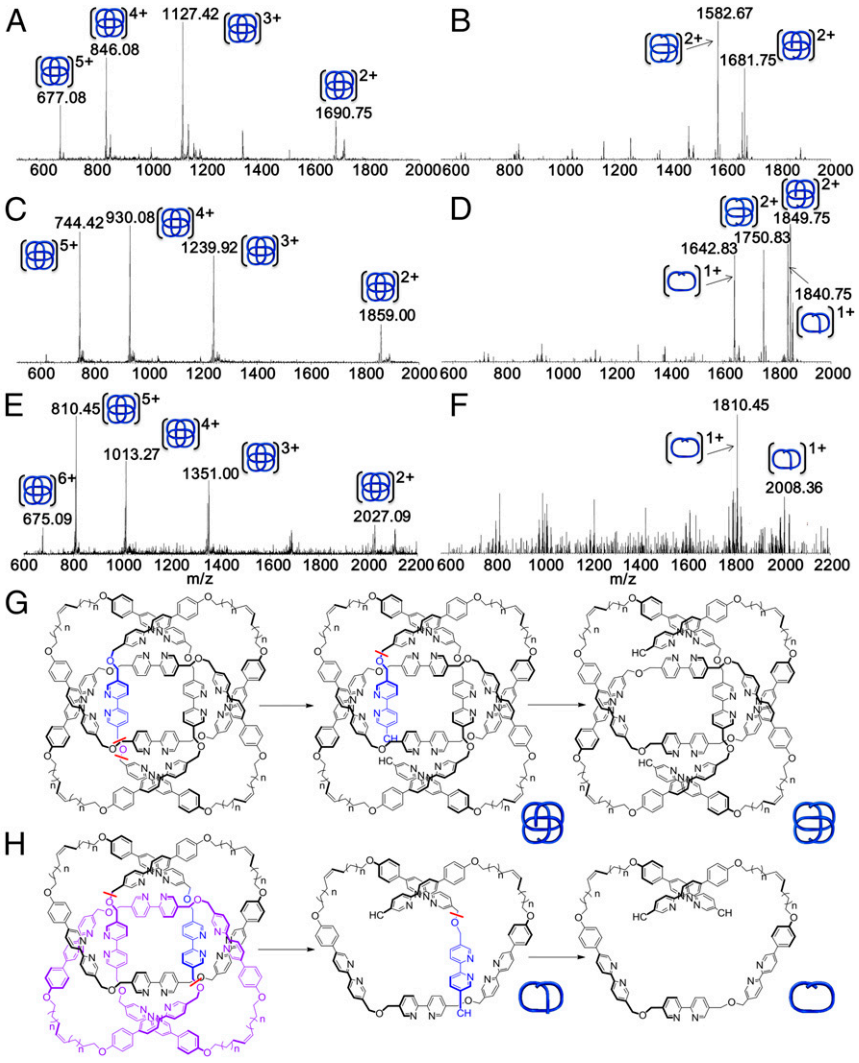

Fig. 4. Fragmentation of 8_{19} knots **1–3** under CID-MS experiments. (*A*) CID-MS of knot **1**. (*B*) MS-MS of $[M+2H]^{2+}$ (m/z = 1,690.75) from knot **1**, only type I fragmentation is observed. (*C*) CID-MS of knot **2**. (*D*) MS-MS of $[M+2H]^{2+}$ (m/z = 1859.00) from knot **2**, both types of fragmentations are observed. (*E*) CID-MS of knot **3**. (*F*) MS-MS of $[M + 2H]^{2+}$ (m/z = 2,027.09) of knot **3**, only type II fragmentation is observed. No fragment ions corresponding to macrocycles, which could arise from molecular links (e.g., a [2]catenane or Solomon link) upon fragmentation of one ring (17), was observed over a range of collision energies, further demonstrating that only knots are present. (*G* and *H*) Two different fragmentation pathways (type I, *G*; type II, *H*) for the 8_{19} knots corresponding to the MS-MS results shown in *B*, *D*, and *E*; bond cleavage is indicated with a red wavy line, the residues lost in the first step are colored purple, and those lost in the second step are colored blue.

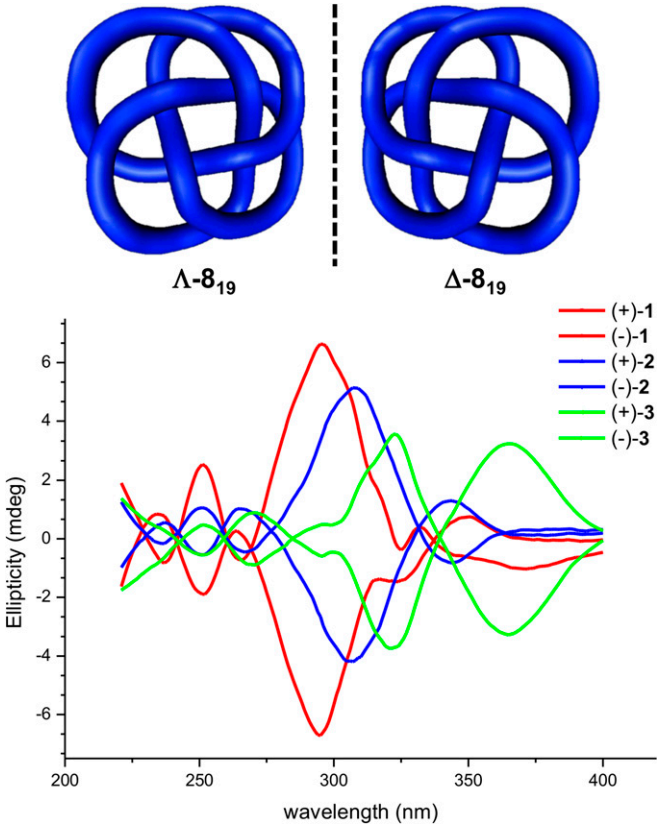

Fig. 5. CD spectra of each enantiomer of molecular 8_{19} knots **1**, **2**, and **3**.

pattern are observed with knot **2** at 35 eV (Fig. 4*D*, m/z = 1,849.75 and 1,750.83 for type I and m/z = 1,840.75 and 1,642.83 for type II). Clearly knot tightness significantly affects covalent bond strength; the tighter the knot, the more easily some bonds can be broken. The experimental results are consistent with the simulations that suggest that tight knotting forces the adoption of conformations with strained bond lengths and angles.

Wiberg bond indices analysis, as implemented in the Gaussian09 suite of programs (35) was conducted with the Minnesota 2006 hybrid meta exchange-correlation functional (M06-2X) (36) and Pople's basis set with polarization functions, 6-31G(d), on the global minimum energy structures of doubly charged **1** and **3** to calculate the bond order of the carbon–oxygen bond between the central bipyridine and phenyl–bipyridine units (C_e–O–C_d, Fig. 1). The calculations on the tightest knot, **1**, show that one of these carbon–oxygen bonds is significantly weaker than others and is more likely to break in the CID-MS experiments (*SI Appendix*, Fig. S38). After cleavage, the resulting terminal oxygen atom can reorganize its electronic structure to allow loss of a water molecule (Fig. 4*G*). In the loosest knot, **3**, the carbon–oxygen bonds all have similar bond orders that are higher than the weak C–O bond in **1**. This can result in near-simultaneous cleavage of two C–O bonds at higher energy (*SI Appendix*, Fig. S38), to produce the two halves of **3** observed experimentally (Fig. 4*H*).

The effect of knot tightness on the spectral properties of **1–3** was also investigated. The UV-vis spectra of knots **1** and **2** are similar, with a slight decrease in absorption at λ_{max} = 306 nm for **2**. However, the absorption of the loosest knot, **3**, decreases significantly and is associated with a 10-nm red shift (*SI Appendix*, Fig. S25). Simulated spectra, generated from time-dependent density functional theoretical (37) calculations at the M06-2X/6–31G(d) level of theory, show that the electronic spectra of the knots are highly sensitive to the two torsional angles, θ_1 and θ_2, within the phenyl–bipyridine moieties (Fig. 3*D* and *SI Appendix*, Figs. S35–S37). The observed red shift of knot **3** is due to the variation of θ_1 and θ_2 as the increased flexibility of the loose knot allows the chromophores to populate more conjugated, flatter, conformations.

An 8_{19} knot is intrinsically chiral by virtue of its topology. The enantiomers of **1–3** were isolated by chiral high-performance liquid chromatography (HPLC) and analyzed by CD spectroscopy (Fig. 5 and *SI Appendix*, Figs. S23 and S24). Each pair of knot enantiomers gives CD spectra of equal but opposite shape and sign (38, 39). As the knots become looser from **1** to **3**, the change in the environment around the chromophores results in a red shift of the CD signal in the spectra of the respective molecules. The simulations and ^{1}H NMR experiments suggest that the bipyridine and phenolic ethers are locked in a chiral conformation in the tightest knot, **1**, which features strong π–π interactions. However, the looser knots have a variety of conformations that average out to give a weaker CD response. The red shift is a consequence of the more conjugated, flat, conformations of the chromophores in the looser knots. The dynamics and conformation of the knotted structures are clearly significantly affected by tightness, with the expression of chirality tunable by tightening or loosening the entanglement.

Analysis of the molecular-dynamics simulations suggests that the property trends observed for 8_{19} knots **1–3** are not a specific consequence of the particular aromatic-ring–based backbones of their structures. Atomic fluctuations measure the flexibility of (large) molecular systems. They are connected to the temperature B factor (40) that can be measured experimentally and is usually reported together with a protein structure in the Protein Data Bank. In the molecular-dynamics simulations, the size of the atomic fluctuations of the aromatic rings, the aliphatic chains, and the entire knot were found to be a function of tightness (Table 1): the tighter the knot, the smaller the fluctuations. The trends are broadly similar for each of the three structural elements monitored (aromatics, aliphatics, and the whole molecule).

The structures of snapshots of the molecular dynamics that successfully simulated the experimental data were used to investigate the interactions between the aromatic fragments and the strain energies of the alkyl chains in the three knots (Table 1). The calculations were performed at the M06-2X/6-31G(d) level of theory. For the interactions between aromatic rings, the correction for basis-set superposition error was determined using the counterpoise method (41). In order of decreasing knot tightness (**1** to **2** to **3**), the average interaction energy between aromatic fragments reduces from −48.3 to −40.1 to −23.6 kcal/mol (Table 1). The variation reflects the greater strand dynamics as the knots become looser. In the same series the average strain energies of the alkyl chains increase from 53.8, 160.0, and 260.1 kcal/mol, as more methylene groups are added to each chain, forced by the knot topology to adopt strained dihedral angles and CH–CH steric clashes. Aromatic stacking interactions do not generate favored conformations in the more flexible knots, but rather form to alleviate strain when the tightness of knotting forces the molecule to become more compact. The stacking of aromatic rings is a consequence of knot tightness rather than the

Table 1. Atomic fluctuations, Δ (Å^2), aromatic fragment interactions, E_{frag} (kcal/mol), and strain energy of the alkyl chain, E_{strain} (kcal/mol), of the three knots (1–3)

Knot	$\Delta_{aromatic\ rings}$	$\Delta_{entire\ knot}$	$\Delta_{alkyl\ chain}$	E_{frag}	E_{strain}
1	2.26	2.31	2.66	−48.3	53.8
2	4.95	5.39	6.86	−40.1	160.0
3	7.43	8.42	10.77	−23.6	260.1

driving force behind its conformation/structure. The aromatic rings in the Tris(2,2′-bipyridine) ligand strands are necessary for the knot synthesis and, in some cases (^{1}H NMR, CD spectra), provide useful probes for the experimental detection of behavior. If π-stacking was the dominating interaction that determined their conformation, the knots would not be the highly dynamic systems that experiments and simulations show them to be. It therefore seems likely that the trends observed for **1–3** are not directly related to their particular molecular make-up but will more generally reflect aspects of behavior regarding knot tightness at the nanoscale.

Conclusions

A series of molecular 8_{19} knots that differ only in the length of alkyl chains that connect rigid aromatic regions enable the investigation of the influence of knot tightness on a range of physical and chemical properties, allowing experimental observations to be rationalized through computational simulations. The tightness of molecular 8_{19} knots affects reactivity (the rate of demetallation of knotted ligands and collision energies required for bond breaking), conformation (rigid regions preferring to be outside the region of entanglement in looser structures), and the expression of topological chirality (manifest in CD and ^{1}H NMR spectra). These results provide some experimental evidence of the effects of tightening knots at the molecular level, which should prove useful in understanding the role of knotting in entangled polymers and in the design of future knotted and interwoven nanomaterials (42–45).

Materials and Methods

Synthesis. Molecular knots **2** and **3** were prepared by modifying the braiding strategy previously used (29) to assemble knot **1** (Fig. 1). Subjecting each metallated knot ($[Fe_4\mathbf{1}](PF_6)_7Cl$, $[Fe_4\mathbf{2}](PF_6)_7Cl$, or $[Fe_4\mathbf{3}](PF_6)_7Cl$) to a 1:1 $MeCN/NaOH_{aq}$ (1 M) solution at 80 °C, followed by size-exclusion chromatography, afforded the corresponding demetallated knots **1–3**, which were characterized by NMR and mass spectrometry. The enantiomers of **1–3** were isolated by chiral HPLC and analyzed by CD spectroscopy.

Molecular-Dynamics Simulations. Molecular-dynamics simulations were carried out with the AMBER 12.0 suite of programs. The knots were parametrized using the general AMBER force field and the standard restrained electrostatic potential procedure carried out to assign charges to atoms by Antechamber. The crystallographic structure of metallated knot $[Fe_4\mathbf{1}]^{8+}$ was used as the starting structure for **1** and as a template for **2** and **3**.

ACKNOWLEDGMENTS. We thank the China 1000 Talents Plan, East China Normal University, the Engineering and Physical Sciences Research Council (EP/P027067/1) and the European Research Council, Advanced Grant 339019 for funding, and the University of Manchester for a President's Doctoral Scholar Award (to L.Z.). D.A.L. is a China 1000 Talents "Topnotch Talent" Professor and Royal Society Research Professor.

1. Sułkowska JI, Rawdon EJ, Millett KC, Onuchic JN, Stasiak A (2012) Conservation of complex knotting and slipknotting patterns in proteins. *Proc Natl Acad Sci USA* 109: E1715–E1723.
2. Wasserman SA, Cozzarelli NR (1986) Biochemical topology: Applications to DNA recombination and replication. *Science* 232:951–960.
3. Tubiana L, Rosa A, Fragiacomo F, Micheletti C (2013) Spontaneous knotting and unknotting of flexible linear polymers: Equilibrium and kinetic aspects. *Macromolecules* 46:3669–3678.
4. Dzubiella J (2009) Sequence-specific size, structure, and stability of tight protein knots. *Biophys J* 96:831–839.
5. Sułkowska JI, Sułkowski P, Szymczak P, Cieplak M (2008) Stabilizing effect of knots on proteins. *Proc Natl Acad Sci USA* 105:19714–19719.
6. Saitta AM, Soper PD, Wasserman E, Klein ML (1999) Influence of a knot on the strength of a polymer strand. *Nature* 399:46–48.
7. Caraglio M, Micheletti C, Orlandini E (2015) Stretching response of knotted and unknotted polymer chains. *Phys Rev Lett* 115:188301.
8. Ziegler F, et al. (2016) Knotting and unknotting of a protein in single molecule experiments. *Proc Natl Acad Sci USA* 113:7533–7538.
9. Alexander JW, Briggs GB (1926) On types of knotted curves. *Ann Math* 28:562–586.
10. Bates A (2005) *DNA Topology* (Oxford Univ Press, Oxford), pp 36–37.
11. Fenlon EE (2008) Open problems in chemical topology. *Eur J Org Chem* 2008: 5023–5035.
12. Gonzalez O, Maddocks JH (1999) Global curvature, thickness, and the ideal shapes of knots. *Proc Natl Acad Sci USA* 96:4769–4773.
13. Orlandini E, Polles G, Marenduzzo D, Micheletti C (2017) Self-assembly of knots and links. *J Stat Mech* 26:034003.
14. Orlandini E, Whittington SG (2007) Statistical topology of closed curves: Some applications in polymer physics. *Rev Mod Phys* 79:611–642.
15. Dai L, van der Maarel JRC, Doyle PS (2012) Effects of nanoslit confinement on the knotting probability of circular DNA. *ACS Macro Lett* 1:732–736.
16. Baiesi M, Orlandini E, Whittington SG (2009) Interplay between writhe and knotting for swollen and compact polymers. *J Chem Phys* 131:154902.
17. Fielden SDP, Leigh DA, Woltering SL (2017) Molecular knots. *Angew Chem Int Ed Engl* 56:11166–11194.
18. Lim NCH, Jackson SE (2015) Molecular knots in biology and chemistry. *J Phys Condens Matter* 27:354101.
19. Dommersnes PG, Kantor Y, Kardar M (2002) Knots in charged polymers. *Phys Rev E Stat Nonlin Soft Matter Phys* 66:031802.
20. Metzler R, Hanke A, Dommersnes PG, Kantor Y, Kardar M (2002) Equilibrium shapes of flat knots. *Phys Rev Lett* 88:188101.
21. Zheng X, Vologodskii A (2010) Tightness of knots in a polymer chain. *Phys Rev E Stat Nonlin Soft Matter Phys* 81:041806.
22. Arteca GA (2007) Externally steered relaxation of tight polyethylene tangles with different initial knot topologies. *Theor Chem Acc* 118:549–556.
23. Mansfield ML (1998) Tight knots in polymers. *Macromolecules* 31:4030–4032.
24. Cantarella J, Kusner RB, Sullivan JM (1998) Tight knot values deviate from linear relations. *Nature* 392:237–238.
25. Katritch V, Olson WK, Vologodskii A, Dubochet J, Stasiak A (2000) Tightness of random knotting. *Phys Rev E Stat Phys Plasmas Fluids Relat Interdiscip Topics* 61: 5545–5549.
26. King NP, Yeates EO, Yeates TO (2007) Identification of rare slipknots in proteins and their implications for stability and folding. *J Mol Biol* 373:153–166.
27. Arai Y, et al. (1999) Tying a molecular knot with optical tweezers. *Nature* 399: 446–448.
28. Orlandini E, Polles G, Marenduzzo D, Micheletti C (2017) Self-assembly of knots and links. *J Stat Mech Theory Exp* 2017:034003.
29. Danon JJ, et al. (2017) Braiding a molecular knot with eight crossings. *Science* 355: 159–162.
30. Garber SB, Kingsbury JS, Gray BL, Hoveyda AH (2000) Efficient and recyclable monomeric and dendritic Ru-based metathesis catalysts. *J Am Chem Soc* 122:8168–8179.
31. Zhang L, et al. (2018) Stereoselective synthesis of a composite knot with nine crossings. *Nat Chem* 10:1083–1088.
32. Meyer M, Albrecht-Gary A-M, Dietrich-Buchecker CO, Sauvage J-P (1997) Dicopper(I) trefoil knots: Topological and structural effects on the demetalation rates and mechanism. *J Am Chem Soc* 119:4599–4607.
33. Orlandini E, Baiesi M, Zonta F (2016) How local flexibility affects knot positioning in ring polymers. *Macromolecules* 49:4656–4662.
34. Poier P, Likos CN, Matthews R (2014) Influence of rigidity and knot complexity on the knotting of confined polymers. *Macromolecules* 47:3394–3400.
35. Frisch MJ, et al. (2009) *Gaussian 09* (Gaussian, Inc., Wallingford, CT).
36. Zhao Y, Truhlar DG (2008) Density functionals with broad applicability in chemistry. *Acc Chem Res* 41:157–167.
37. Adamo C, Jacquemin D (2013) The calculations of excited-state properties with time-dependent density functional theory. *Chem Soc Rev* 42:845–856.
38. Rapenne G, Dietrich-Buchecker C, Sauvage J-P (1996) Resolution of a molecular trefoil knot. *J Am Chem Soc* 118:10932–10933.
39. Vögtle F, et al. (2001) Novel amide-based molecular knots: Complete enantiomeric separation, chiroptical properties, and absolute configuration. *Angew Chem Int Ed* 40:2468–2471.
40. Frauenfelder H, Petsko GA, Tsernoglou D (1979) Temperature-dependent X-ray diffraction as a probe of protein structural dynamics. *Nature* 280:558–563.
41. Boys SF, Bernardi F (1970) The calculation of small molecular interactions by the differences of separate total energies. Some procedures with reduced errors. *Mol Phys* 19:553–566.
42. Liu Y, et al. (2016) Weaving of organic threads into a crystalline covalent organic framework. *Science* 351:365–369.
43. Marcos V, et al. (2016) Allosteric initiation and regulation of catalysis with a molecular knot. *Science* 352:1555–1559.
44. Lewandowska U, et al. (2017) A triaxial supramolecular weave. *Nat Chem* 9: 1068–1072.
45. Wang Z, et al. (2017) Molecular weaving via surface-templated epitaxy of crystalline coordination networks. *Nat Commun* 8:14442.